Three-dimensional mapping of lingual myoarchitecture by diffusion tensor MRI[†]

Sungheon Kim,[1]* Alan S. Barnett,[2‡] Carlo Pierpaoli[3‡] and Gloria Chi-Fishman[4‡]

[1]Department of Radiology, University of Pennsylvania, Philadelphia, USA
[2]National Institute of Mental Health, National Institutes of Health, Bethesda, MD, USA
[3]National Institute of Child Health and Human Development, National Institutes of Health, Bethesda, MD, USA
[4]Physical Disabilities Branch, Department of Rehabilitation Medicine, Clinical Research Center, National Institutes of Health, Bethesda, MD, USA

ABSTRACT: This study was performed to assess the feasibility of investigating the complex lingual myoarchitecture through segmentation of muscles from diffusion tensor imaging (DTI) data. The primary eigenvectors were found to be adequate for delineating the superior and inferior longitudinalis, genioglossus, and hyoglossus. The tertiary eigenvector orientations effectively revealed the homogeneous and systematic change of muscle orientation in the tongue core. In the longitudinalis near the tongue tip, the secondary eigenvectors were oriented in the radial direction. Lingual muscles were segmented using two methods: modified directional correlation (DC) and tensor coherence (TC) methods. The DC method, based on one eigenvector, was found to be inadequate for lingual muscle segmentation, whereas the TC method, based on the tensor shape and orientation, was used successfully to segment most lingual muscles. The segmentation result was used to report the diffusion tensor properties of individual lingual muscles. Also found was a continuous change in skewness of the intrinsic tongue core from negative in the anterior region to positive in the posterior region. DTI and the proposed segmentation method provide an adequate means of imaging and visualizing the complex, compartmentalized musculature of the tongue. The potential for *in vivo* research and clinical applications is demonstrated. Copyright © 2007 John Wiley & Sons, Ltd.

KEYWORDS: diffusion tensor imaging; tongue; muscle; segmentation; lingual myoarchitecture

INTRODUCTION

The tongue has a myoarchitecture that is unparalleled in complexity by any other organs in the human body. It is diverse in function and plays crucial roles in speech production and swallowing. Despite the importance of its function in daily living, human lingual myoarchitecture has not been investigated rigorously to date. The twentieth century saw only a limited number of empirical descriptions of the tongue musculature. The morphology of the human tongue was described by Abd-el-Malek in 1939 (1) based on transverse sections only. In 1974,

Miyawaki (2) presented a series of human tongue illustrations from serial sections in sagittal, coronal, and transverse planes, which described in detail four intrinsic (superior longitudinalis, inferior longitudinalis, transversus, and verticalis) and three extrinsic (genioglossus, hyoglossus, and styloglossus) muscles in this unique organ that has no bones or joints. The intrinsic muscles originate and insert within the tongue to form a complex 3D mesh; the extrinsic muscles all have bony origins but soft tissue insertions into the tongue. Similar muscle groups have been identified in other mammals such as dog (3), pig (4), cow (5), and sheep (6). Although the interdigitation of the transverse and vertical muscle fibers had been noted earlier, it was not until 2001 that, through Takemoto's gross dissection of the human tongue into wedge-shaped blocks followed by serial sections parallel to the tongue surface (7), we gained a more detailed perspective on the manner of interdigitation of these muscles as serially repeating pairs of thin muscle fiber laminae, with the transversus as one pair and mixed genioglossus–verticalis as the other pair. These historical and modern histological studies clearly show that different perspectives may be gained from different dissection strategies, and that an adequate understanding

of the complex lingual myoarchitecture requires a detailed three-dimensional (3D) analytical approach that is difficult to undertake through histological sections.

Diffusion tensor imaging (DTI) was recently introduced as a tool to image organized fibrous tissue microstructures (8), based on the fact that NMR signals can be made sensitive to the random motion of water molecules in biological tissues (9). DTI has been extensively used to study the central nervous system and to detect changes due to neurological diseases (10). It has also been used to study skeletal (8,11) and cardiac (12) muscles and found to provide useful information on muscle fiber orientation for biomechanical studies of muscle function. Gilbert *et al*. (6) made the first attempt to use DTI to study lingual myoarchitecture and demonstrated a qualitative agreement between anisotropic water diffusion and histological observation of muscle fibers in *ex vivo* sheep tongues. Since then, the feasibility of using DTI to study the lingual myoarchitecture has been evaluated and documented (4,5,13–15).

Although these studies have demonstrated the potential of DTI in revealing the complex arrangement of lingual muscle fibers, segmentation of lingual muscles using DTI has not been reported to our knowledge. Individual lingual muscles appear to be well localized in DTI maps. However, reliable segmentation of lingual muscles remains a challenging task, as the boundary between the muscles is often not clear because of complex intertwining of muscle fibers. Automatic or semi-automatic segmentation of lingual muscles can be a useful tool to perform quantitative analysis of lingual muscles for basic science and clinical research in crucial tongue functions such as swallowing and speech. The purpose of this study was to develop a segmentation method for 3D lingual morphological analysis in an excised calf tongue model.

MATERIALS AND METHODS

Specimens

The experiments were performed with three excised unembalmed calf tongues obtained from a USDA-approved commercial slaughterhouse. The specimens were excised by *en bloc* resection less than 2 h after the animals were slaughtered. They were enclosed in polyethylene wrap to avoid dehydration, sealed in a rectangular plastic container, and refrigerated. The specimens were warmed to room temperature before MR scanning. All specimens were scanned within 24 h of harvest.

MR data acquisition and processing

DTI was performed on the fresh specimens using a 1.5 T GE Signa MR scanner (GE Medical Systems, Milwaukee,

WI, USA) equipped with a whole-body gradient coil producing gradient pulses up to 50 mT/m, and a 20 cm receive–transmit head coil. To minimize the effect of susceptibility and relatively short T_2 in muscle tissue, we applied a diffusion-sensitive stimulated-echo acquisition mode (STEAM) pulse sequence with eight-shot echo-planar spatial encoding. The acquisition matrix was 128×64, the field of view was $260\,mm \times 130\,mm$, and the slice thickness was 2 mm, yielding a spatial resolution of $2.03 \times 2.03 \times 2\,mm^3$. The image acquisition was repeated eight times to improve signal-to-noise ratio (SNR). The acquisition included 50 axial slices to cover the entire tongue without gap. The *TR* was 16.0 s; it was kept long enough to scan the prescribed number of slices without overloading the gradient amplifier during the long scan. A conventional scheme of six non-collinear gradient vector directions was chosen for diffusion weighting: $[1,1,0]$, $[1,0,1]$, $[0,1,1]$, $[1,-1,0]$, $[1,0,-1]$, and $[0,1,-1]$. To minimize the cross-term effect and any bias, the opposite directions were also used, resulting in 12 gradient weighting directions, plus non-weighting, $[0,0,0]$. The diffusion gradient was 44.5 mT/m in amplitude, 3.5 ms in duration, and 400 ms in separation, yielding 1400 s/mm^2 effective diffusion weighting when the gradients on two axes were turned on. The total scan time was ∼7 h 30 min. Diffusion-weighted images were co-registered to non-diffusion-weighted images using a multi-channel registration method (16) to correct for the eddy current effects. The diffusion tensors were estimated using a non-linear fitting method with noise estimation to minimize the effect of noise (17). The directionally encoded color (DEC) mapping method (18) was used to show the muscle fiber orientations. DEC maps of the primary and tertiary diffusion tensor eigenvectors contained the most meaningful information and hence were used to visualize the 3D morphology of unidirectional muscles as well as the interdigitation of muscle fibers in the tongue core. The image reconstruction was performed using software written in IDL (ITT Visual Information Solutions, Boulder, CO, USA).

Segmentation of muscular compartments of the tongue

A novel semi-automatic segmentation method was developed based on a concept similar to the directional correlation (DC) method, which was first used to segment white matter tracts in the rat brain (19) and recently in the human brain (20). The DC method groups anisotropic voxels based on the normalized inner product of their primary eigenvectors, starting from manually selected seed points. Newly grouped voxels then become the new starting points for iterative region-growing until there are no more neighboring voxels to include in the group. Although this method has been demonstrated to work reasonably well for the white matter tracts, its use is

limited to the linear anisotropic regions because it utilizes the primary eigenvector orientation only. This method may not be an appropriate choice for the tongue muscles, because not all the tongue muscles can be identified with high linear anisotropy. One of the major parts of the tongue musculature is the intrinsic core region, which has alternating layers of verticalis and transversus muscles (7). As mentioned in the previous section, previous DTI studies (4,5,14) showed that the interwoven configuration of these two muscles was responsible for the oblate (planar anisotropic) diffusion tensor found in the tongue core. For an oblate tensor, the sorting of the primary and secondary eigenvectors can be greatly affected by noise. Hence, a modification of the original DC method is necessary for tongue muscle segmentation.

To overcome this issue, the conventional DC method was extended in two different ways: modified DC and tensor coherence (TC) methods. In the modified DC method, the primary eigenvector was used for linear-anisotropic muscles (genioglossus, geniohyoid, hyoglossus, and longitudinalis) and the tertiary eigenvector for planar-anisotropic muscle (tongue core). As the styloglossus was not fully retained in the excised tongue specimen, segmentation of this muscle was not attempted. The readily visible geniohyoid, on the other hand, was included to augment the feasibility assessment for our segmentation methodology, as activities of this suprahyoid muscle are often synergistic with, and inseparable from, those of the lingual muscles for many functional oral movements. It was assumed that the tertiary eigenvector of the tongue core represented the normal direction to the plane containing both transversus and verticalis muscles. DC was defined as

$$DC_n(D_i, D_j) = \varepsilon_{in} \cdot \varepsilon_{jn} \qquad [1]$$

where ε_{in} represents the nth eigenvector of diffusion tensor D_i at pixel i. The second approach was to segment lingual muscle groups on the basis of both tensor orientation and shape. The similarity in orientation and shape was estimated by TC defined as the normalized inner product of the anisotropic part of the diffusion tensors:

$$TC(D_i, D_j) = \frac{D_i : D_j}{\sqrt{D_i : D_i}\sqrt{D_j : D_j}} \qquad [2]$$

where

$$D_i : D_j$$
$$= \sum_{m=1}^{3}\sum_{n=1}^{3}\left(\sqrt{\lambda_{im}}\varepsilon_{im} \cdot \sqrt{\lambda_{jn}}\varepsilon_{jn}\right)^2$$
$$- Trace(D_i)Trace(D_j)/3 \qquad [3]$$

λ represents eigenvalues, and ε represents eigenvectors. The similarity of diffusion tensors based on the tensor scalar product has been used for white matter tract segmentation (21).

The iterative region-growing process began from manually selected multiple seed points within a muscle and continued until there was no more voxel to include in the group. There were two inclusion criteria for a new voxel: fractional anisotropy (22) larger than 0.15, and DC (or TC) larger than a threshold value. As lingual muscles are located close to each other, choosing the right threshold value is critical for successful segmentation. In our study, we investigated the relationship between the number of recruited voxels and the threshold as the threshold was varied gradually from 0.99 to 0.7 for DC (equivalent to angular distance of 45°) and from 0.98 to 0.5 for TC. As the lingual muscles have only narrow gaps between them or are attached to each other, it was expected that lowering the threshold would eventually lead the region-growing process to enter the neighboring muscles, which may cause a sudden increment in the number of recruited voxels. In the profile of the number of recruited voxels as a function of DC or TC, the sudden-increment point (SIP) was defined as the point where the increment is more than twice that of the previous step during the systematic evaluation from high DC or TC values to low values. Before application of the segmentation, the raw data were regularized by a $3 \times 3 \times 3$ Gaussian filter with $\sigma = 1.0$. The segmentation result was used to generate a 3D rendering of the lingual myostructure. The segmentation and rendering were implemented using MATLAB (The MathWorks, Inc., Natick, MA, USA).

RESULTS

Compartmentalized lingual muscles

Figure 1 presents the axial, sagittal, and coronal views of a representative multi-slice DTI dataset of the calf tongue. The tongue core, with its interwoven fibers of verticalis and transversus muscles, is clearly visualized (in randomly distributed green and red patches) and is surrounded by the longitudinalis muscles (blue) in axial (Fig. 1b, ax1), sagittal (Fig. 1c, sg2), and all coronal images (Fig. 1d, cr1–cr10). The planes containing crossing muscle fibers appear to be oriented consistently parallel to one another, making the tertiary eigenvector orientations highly homogeneous, as shown in the tertiary eigenvector DEC maps of Fig. 1f. The systematic changes in the orientation of the fiber-crossing planes can be seen in all panels of Fig. 1, especially the coronal images in Fig. 1d–f. In our chosen orientation of the tongue, planes containing crossing vertical and transverse muscle fibers are initially coronal, extending from the anterior tip to about the middle of the tongue (cr1–6). From mid tongue to the tongue base (cr7–10), the planes begin to slowly rotate and eventually become almost axial, as illustrated in the changing colors of the intrinsic tongue core from blue to green in Fig. 1f.
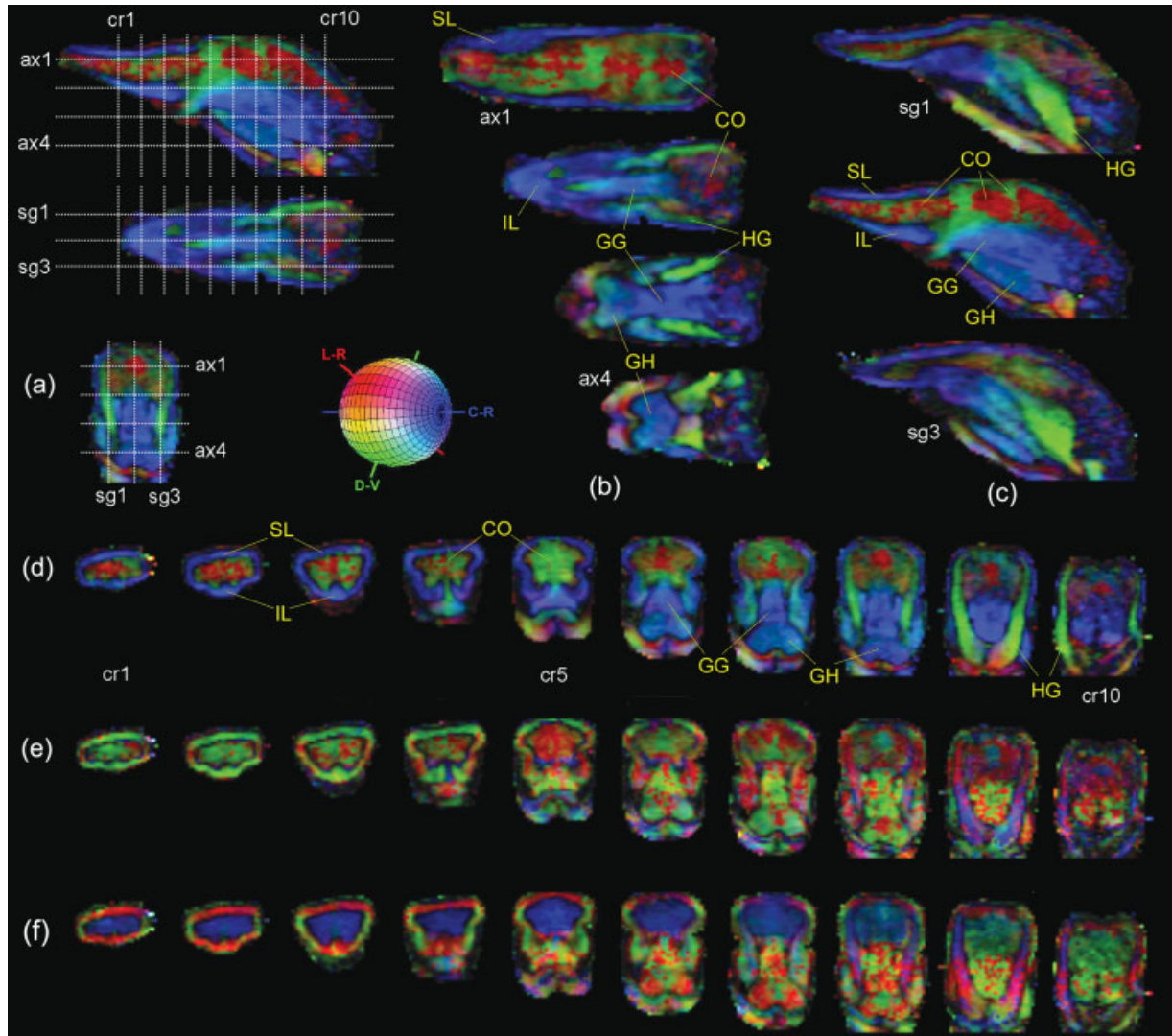
Figure 1. DEC maps based on primary (a–d), secondary (e), and tertiary (f) eigenvector orientations weighted by lattice index. (a) Slice locations superimposed on sagittal (sg), axial (ax), and coronal (cr) images; (b) axial images; (c) sagittal images; (d–f) coronal images. The color code corresponds to the directions shown in the color globe: red for left–right (L–R), green for dorsal–ventral (D–V), and blue for caudal–rostral (C–R) directions. Note that the colors in (f) represent the tertiary eigenvector direction, not the direction of the muscles. GG, genioglossus; GH, geniohyoid; HG, hyoglossus; CO, intrinsic core; SL, superior longitudinalis; IL, inferior longitudinalis.

Fibers of the superior and inferior longitudinalis muscles are clearly delineated in the sagittal images (sg1–3) as blue bands above and below the anterior tongue core, as shown in Fig. 1c. The longitudinal fibers enwrap the core region in the entire anterior tongue, and it can be seen that there is no distinguishable boundary between the two longitudinalis muscles at the lateral margins on the basis of their diffusivity characteristics (cr1–5 in Fig. 1d). Bilaterally, the inferior longitudinalis muscle divides into two sections, as the genioglossus and geniohyoid muscles merge into the tongue body (cr4–5 in Fig. 1d). The primary eigenvectors are homogeneously oriented in a longitudinal direction shown in blue in Fig. 1d. In contrast, the secondary eigenvectors of the longitudinalis near the tongue tip are oriented in a radial direction as shown in Fig. 1e.

The genioglossus is also clearly delineated, appearing green and blue in the mid-sagittal image (sg2) and predominantly blue in the center of the mid-axial images (ax2–3) and below the tongue core in some of the coronal images (cr5–10 in Fig. 1d). The hyoglossus muscle is visualized on the lateral borders of the tongue in green, as shown in the parasagittal images (sg1 and sg3 in Fig. 1c) and the posterior coronal images (cr8 and cr9 in Fig. 1d). It originates from the hyoid bone bilaterally and radiates into the longitudinalis muscles. The styloglossus was difficult to identify because of the lack of clear anatomical landmarks based on diffusivity characteristics to indicate its insertion path and pattern into the tongue. From the lingual anatomy of humans (2,7) and horses (23), it is likely that the distinct bilateral fiber bundle in the region ventrolateral to the hyoglossus not only contains fibers of

the longitudinalis muscles but is also the insertion region of the styloglossus muscle.

Segmentation using DC

Segmentation of the lingual muscles was performed using the modified DC method in which DC was calculated from the tertiary eigenvectors for the intrinsic tongue core and from the primary eigenvectors for the other muscles. Figure 2 shows the number of voxels segmented for each muscle using DC as the DC threshold level systematically lowered in 0.01 increments from 0.99 to 0.7. In the case of the tongue core as shown in Fig. 2a, it was possible to detect at least one SIP for each specimen as indicated by the arrows. However, for the genioglossus (Fig. 2b), geniohyoid (Fig. 2c), and longitudinalis (Fig. 2d), there was at least one specimen in each case where it was difficult to detect a step increment. In the case of the genioglossus and geniohyoid, visual inspection of the pixel maps of recruited voxels showed that the voxels selected with DC > 0.99 already represented the areas larger than expected for these muscles. For the long-

itudinalis, a SIP was only detectable in specimen 2, and not in the other specimens. It was further noted that the number of voxels for specimen 1 was already substantially higher than that of specimen 2 at SIP. Thus, DC = 0.99 was used as the threshold value for those cases without detectable SIP. Segmentation using DC appeared to be most effective for the hyoglossus, as it was easy to determine SIP for all three specimens as shown in Fig. 2e and 2f.

The segmentation results for specimen 1 are depicted in volume-rendered images in Fig. 3a. The top panel shows the genioglossus (in purple) extending all the way to the back of the tongue. This may primarily be due to the fact that the genioglossus enters the intrinsic tongue core in the direction parallel to the verticalis. Similar to the case of the genioglossus, which emerges into the tongue core, the segmented hyoglossus (in green) also appears to extend into the tongue core. The segmented tongue core is shown in red. It can be seen that the posterior portion of the tongue core is missing, as the genioglossus is shown instead. In general, the results presented in Fig. 2 and Fig. 3a suggest that it is difficult to determine the DC threshold value for the genioglossus, geniohyoid, and
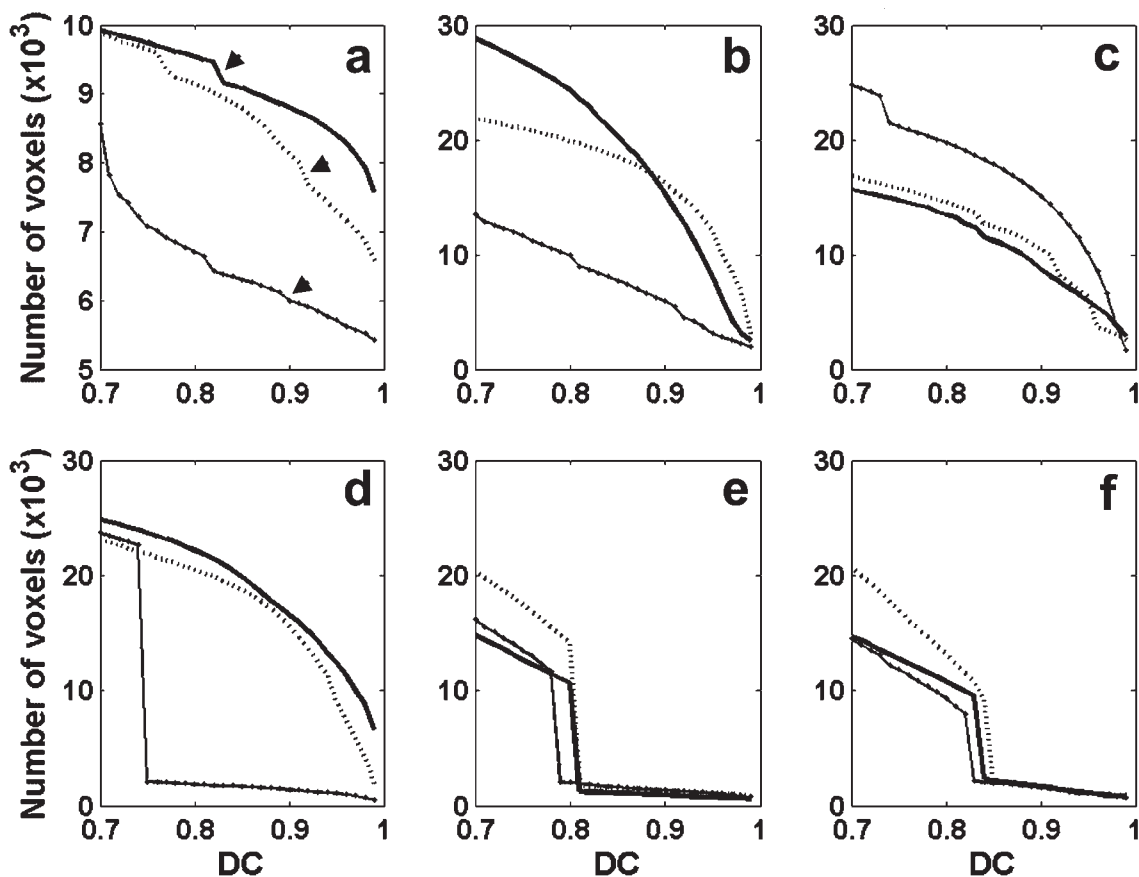
Figure 2. Number of segmented voxels per muscle depending on the threshold level of DC. Segmentation was performed for six lingual muscles: tongue core (a), genioglossus (b), geniohyoid (c), longitudinalis (d), left hyoglossus (e), and right hyoglossus (f). Each panel shows the results from three specimens: thick solid line for specimen 1; thin solid line for specimen 2; dotted line for specimen 3. DC = 0.71 corresponds to 45° between two eigenvectors.
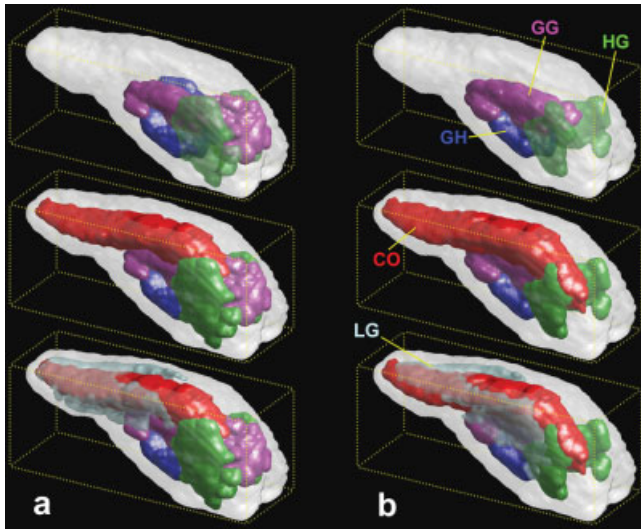
Figure 3. 3D rendering of lingual muscles segmented using DC(**a**) and TC(**b**). The tongue surface is shown in a translucent white color in all panels, with the genioglossus (GG) in purple, geniohyoid (GH) in blue, and hyoglossus (HG) in green. The tongue core (CO), shown in red, includes as a single mass the interwoven verticalis and transversus muscles as well as the genioglossus fibers that have entered the intrinsic tongue. The longitudinalis muscle (LG) is depicted in cyan. Composites of all segmented muscle groups are shown in the bottom row.

longitudinalis. Furthermore, for a muscle emerging into another one, such as the genioglossus and hyoglossus, the segmented muscle appears to be larger than the expected area.

Segmentation using TC

Figure 4 shows the number of voxels segmented for each muscle using TC as the TC threshold level systematically lowered in 0.02 increments from 0.98 to 0.5. For the tongue core as shown in Fig. 4a, specimen 1 did not have any notable SIP, whereas specimens 2 and 3 had a SIP as indicated by the arrows. Visual inspection of the selected voxels with TC > 0.5 from specimen 1 revealed that most voxels represented the tongue core. For the hyoglossus as shown in Fig. 4e and 4f, specimen 1 did not show any SIP for both the right and left sides, whereas specimen 3 had SIPs located close to TC = 0.5. Thus, where it was not possible to detect a SIP, the TC threshold was set to 0.5. For the genioglossus (Fig. 4b), geniohyoid (Fig. 4c), and longitudinalis (Fig. 4d), it was possible to determine appropriate TC threshold levels for all three specimens as indicated by the arrows.
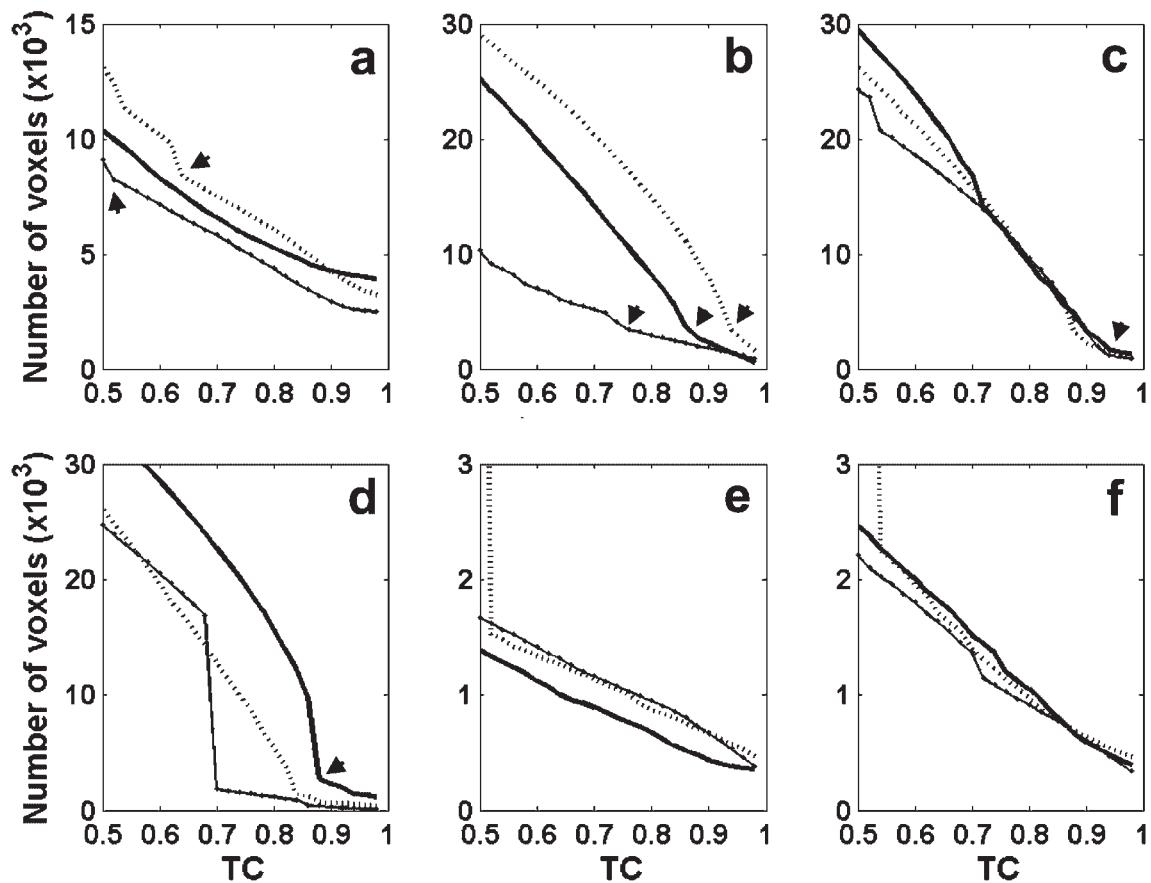
Figure 4. Number of segmented voxels per muscle depending on the threshold level of TC. Segmentation was performed for six lingual muscles: tongue core (a), genioglossus (b), geniohyoid (c), longitudinalis (d), left hyoglossus (e), and right hyoglossus (f). Each panel shows the results from three specimens: thick solid line for specimen 1; thin solid line for specimen 2; dotted line for specimen 3.

The results of segmentation using TC for specimen 1 are shown as volume-rendered images in Fig. 3b. The genioglossus (in purple) in the top panel shows that the segmentation based on TC did not extend into the tongue base, probably because of the change in diffusion tensor shape. The hyoglossus (in green) also did not extend into the tongue core. In the mid panel, it is shown that the posterior region of the tongue core (in red) was successfully segmented without extending to the other neighboring muscles. However, the longitudinalis (in cyan) did not include its lateral and inferior parts, as the region of interest for the seed points was selected in the superior longitudinalis region. Thus, it was found that segmentation using TC provided a reasonable result for most muscles except the longitudinalis in all three specimens.

Segmented lingual muscles

The segmentation results from the TC method were used to measure the diffusivity of individual muscles or muscle groups, as presented in Table 1. The genioglossus, geniohyoid, and hyoglossus muscles were noted to have a similar range of diffusivities and anisotropies. The longitudinalis muscles, as a group, had a large deviation, as they are distributed in a wide area and mixed with many other muscles in various degrees. The intrinsic tongue core could be uniquely identified with a smaller primary eigenvalue and larger secondary eigenvalue. The intrinsic tongue core also displayed a slow variation in the shape of the diffusion tensor along the longitudinal direction (from the tongue tip to the posterior region), as shown in Fig. 5a. This variation, particularly in the secondary eigenvalue, led to a change from negative skewnesses in the tongue tip and mid-tongue region to positive skewnesses in the posterior region, as shown in Fig. 5b.

DISCUSSION

Comparison with previous studies on lingual myoarchitecture

High-resolution DTI was successfully performed to demonstrate the potential of this imaging modality as a tool to visualize lingual muscular architecture. The morphological details of lingual muscles shown by our DEC maps (Fig. 1) are consistent with known gross anatomical features of animal (3) or human (1,2,7) tongues and the results of previous DTI studies of animal tongues (5,6). To our knowledge, extensive histological studies on the 3D morphology of lingual muscles and their fiber orientations have been limited to the post-mortem human tongue (1,2,7). However, Baggett and Doran (24) reported that mammalian species that use their tongues for intraoral mastication share gross lingual structural and functional similarities, in contrast with species that use their tongues for extraoral gathering of food. Our DTI results for the calf tongue also showed a gross myoarchitecture similar to that of the human tongue. Our segmentation using TC successfully visualized the 3D shapes and locations of the lingual muscles. The segmentation results can be directly used to build a finite element model of lingual myoarchitecture for various biomechanical studies, similar to the earlier attempts for skeletal (11) and cardiac (12) muscles.

One might argue that the present study could have used DTI fiber tracking methods to segment selected tongue regions where the muscle fibers are regularly aligned to form high diffusion anisotropy. Gilbert et al. (14) reported fiber tracking results for cow tongue and demonstrated how 3D visualization of the reconstructed fibers could help us to understand the complex arrangement of lingual muscles. However, it is not clear what the reconstructed

Table 1. Eigenvalues ($\times 10^{-6}$ mm^2/s) and fractional anisotropy (FA) of diffusion tensors in the lingual muscles segmented using TC method. Values are mean $\pm$ SD

Specimen	Genioglossus	Geniohyoid	Hyoglossus	Core	Longitudinalis
1					
λ_1	1168 ± 84	1095 ± 71	1171 ± 103	879 ± 78	984 ± 140
λ_2	618 ± 44	657 ± 36	645 ± 54	718 ± 64	650 ± 64
λ_3	541 ± 43	563 ± 37	533 ± 51	523 ± 60	521 ± 56
FA	0.41 ± 0.06	0.35 ± 0.05	0.41 ± 0.07	0.25 ± 0.06	0.32 ± 0.09
2					
λ_1	1137 ± 80	1003 ± 84	1132 ± 95	771 ± 89	905 ± 150
λ_2	540 ± 39	576 ± 33	534 ± 42	611 ± 76	558 ± 59
λ_3	475 ± 39	506 ± 33	459 ± 45	428 ± 52	449 ± 53
FA	0.47 ± 0.05	0.37 ± 0.06	0.48 ± 0.06	0.28 ± 0.06	0.35 ± 0.11
3					
λ_1	1056 ± 44	997 ± 47	1109 ± 75	815 ± 80	878 ± 75
λ_2	599 ± 40	555 ± 39	588 ± 45	743 ± 60	473 ± 67
λ_3	516 ± 41	468 ± 44	494 ± 40	471 ± 57	259 ± 50
FA	0.38 ± 0.05	0.40 ± 0.04	0.43 ± 0.05	0.27 ± 0.07	0.53 ± 0.06
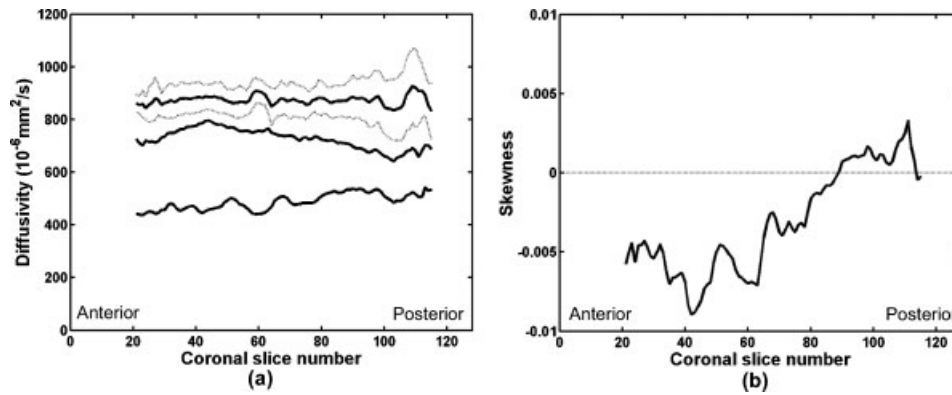
Figure 5. The diffusivity and skewness of the segmented tongue core (specimen 1) vary depending on the coronal slice location. (a) Mean eigenvalues of the segmented tongue core region in each coronal slice are plotted as solid lines. The dotted lines represent the standard deviations for the largest eigenvalues. The standard deviations of the other eigenvalues were smaller than those of the largest eigenvalues. (b) The skewness of the mean eigenvalues shows variation in diffusion tensor shape, changing from oblate (negative skewness) to prolate (positive).

streamlines represent. Unlike the axonal projections of neurons, muscles do not comprise long projections of fibers from one end to another. Individual muscle fibers do not necessarily start from the muscle origin and end at the insertion point. There could be more muscle fibers added in the middle of a muscle depending on the need to generate biomechanical force. Thus, segmentation of muscle fibers with high TC, as demonstrated in this study, appears more intuitively relevant than tractography for the muscles under study.

Complexity in the structure of longitudinalis muscles

Our results clearly show the radial orientation of the secondary eigenvectors of the longitudinalis muscles, in addition to the longitudinal (anterior–posterior) orientation of their primary eigenvectors. This finding is comparable to the report of DePaul and Abbs (25) that the fibers of the verticalis fan out vertically into the superior and inferior longitudinal muscles, and those of the transversus fan out horizontally and bilaterally to terminate in the longitudinal muscles. This is one possible reason why the segmentation result using TC failed to represent the lateral and inferior parts, as the longitudinalis muscle comprises heterogeneous voxels corresponding to different diffusion tensor shapes and orientations.

Optimizing DTI acquisition and analysis for myoarchitecture

Previous studies revealed that the primary eigenvector reflects the muscle fiber orientation. Holmes *et al.* (12) reported that, in the myocardium, the angular difference

between the fiber orientation measured from DTI and histological measurement was about $3.7°$ on the average. Damon *et al.* (26) found a similar degree of high correlation between DTI and histological observations in skeletal muscles. Although these studies suggest the feasibility of using DTI to estimate muscle fiber orientation, caveats exist, as the uncertainty in the estimation of primary eigenvector orientation can be considerably affected by anisotropy (27) and noise level (22). In muscle fibers in particular, it has been shown that the anisotropy of diffusion tensor in muscle decreases with the decrease in allowed diffusion time during data acquisition (28). These investigations point out that the accuracy in the estimation of fiber orientation using DTI can vary, depending on the background noise and imaging condition. In this study, we used 400 ms for diffusion time to maximize the effect of restricted diffusion to achieve high anisotropy. To minimize the bias from the magnitude sorting of principal components and its orientation uncertainty, we also used TC to segment muscles. It is demonstrated that this method is adequate for segmenting muscles with unidirectional fibers as well as two crossing fibers, such as those in the tongue core.

Technical challenges to *in vivo* human study

Within the confines of current imaging technologies, the application of DTI for the *in vivo* study of the human tongue faces several serious challenges, as demonstrated by a recent DTI investigation (13). In addition to the apparent demand for higher-resolution image acquisition, there are a number of issues to address in DTI. One of the problems is the susceptibility artifact due to the air space around the tongue. This study has shown that segmented

echo-planar imaging can minimize the susceptibility artifact. External passive or active coils can also minimize the magnetic field distortion, as demonstrated for the inferior frontal areas in brain imaging (29). Either method or a combination of the two may provide a solution. Another major problem is the MRI scan time. As the tongue is innately involved in various voluntary and involuntary oral movements, it is difficult to hold it in a fixed position for an extended length of time. Scan time must be substantially reduced for *in vivo* imaging of the human tongue while keeping a high enough resolution. The recent development of parallel imaging (30) may offer a means to shorten the scan time to a practically acceptable level. A customized, flexible, multi-channel coil that provides superior SNR will permit parallel imaging and further improve image quality. Clinical imaging of the human tongue will depend on successful implementation of these technical advances.

This study presents evidence that DTI and the proposed analysis method can adequately image and visualize the complex, compartmentalized musculature of the tongue. Our DTI-based 3D model of lingual morphology in intact specimens suggests that this general investigative direction may eventually lead to a better understanding of the relations *in vivo* between the structure and function of the human tongue. Coupled with technical advances that significantly reduce scan time, minimize susceptibility artifacts, and increase SNR and field homogeneity, DTI holds great promise for *in vivo* detection of morphological changes induced by disease, aging, or exercise.

Acknowledgements

REFERENCES

1. Abd-el-Malek S. Observations on the morphology of the human tongue. *J Anat* 1939; **73**: 201–210.
2. Miyawaki K. A study on the musculature of the human tongue: observations on transparent preparations of serial sections. *Ann Bull of RILP, University of Tokyo* 1974; **8**: 23–49.
3. Mu L, Sanders I. Neuromuscular organization of the canine tongue. *Anat Rec* 1999; **256**(4): 412–424.
4. Napadow VJ, Chen Q, Mai V, So PT, Gilbert RJ. Quantitative analysis of three-dimensional-resolved fiber architecture in heterogeneous skeletal muscle tissue using NMR and optical imaging methods. *Biophys J* 2001; **80**(6): 2968–2975.
5. Wedeen VJ, Reese TG, Napadow VJ, Gilbert RJ. Demonstration of primary and secondary muscle fiber architecture of the bovine tongue by diffusion tensor magnetic resonance imaging. *Biophys J* 2001; **80**(2): 1024–1028.
6. Gilbert RJ, Reese TG, Daftary SJ, Smith RN, Weisskoff RM, Wedeen VJ. Determination of lingual myoarchitecture in whole tissue by NMR imaging of anisotropic water diffusion. *Am J Physiol* 1998; **275**(2 Pt 1): G363–369.
7. Takemoto H. Morphological analyses of the human tongue musculature for three-dimensional modeling. *J Speech Lang Hear Res* 2001; **44**(1): 95–107.
8. Basser PJ, Mattiello J, LeBihan D. MR diffusion tensor spectroscopy and imaging. *Biophys J* 1994; **66**(1): 259–267.
9. Stejskal EO, Tanner JE. Spin diffusion measurements: spin echoes in the presence of a time-dependent field gradient. *J Chem Phys* 1965; **42**: 288–292.
10. Le Bihan D, Mangin JF, Poupon C, Clark CA, Pappata S, Molko N, Chabriat H. Diffusion tensor imaging: concepts and applications. *J Magn Reson Imaging* 2001; **13**(4): 534–546.
11. Van Donkelaar CC, Kretzers LJ, Bovendeerd PH, Lataster LM, Nicolay K, Janssen JD, Drost MR. Diffusion tensor imaging in biomechanical studies of skeletal muscle function. *J Anat* 1999; **194**(Pt 1): 79–88.
12. Holmes AA, Scollan DF, Winslow RL. Direct histological validation of diffusion tensor MRI in formaldehyde-fixed myocardium. *Magn Reson Med* 2000; **44**(1): 157–161.
13. Gilbert RJ, Napadow VJ. Three-dimensional muscular architecture of the human tongue determined *in vivo* with diffusion tensor magnetic resonance imaging. *Dysphagia* 2005; **20**(1): 1–7.
14. Gilbert RJ, Magnusson LH, Napadow VJ, Benner T, Wang R, Wedeen VJ. Mapping complex myoarchitecture in the bovine tongue with diffusion spectrum magnetic resonance imaging. *Biophys J* 2006; **91**: 1014–1022.
15. Gilbert RJ, Wedeen VJ, Magnusson LH, Benner T, Wang R, Dai G, Napadow VJ, Roche KK. Three-dimensional myoarchitecture of the bovine tongue demonstrated by diffusion spectrum magnetic resonance imaging with tractography. *Anat Rec A Discov Mol Cell Evol Biol* 2006; **288**(11): 1173–1182.
16. Rohde GK, Barnett AS, Basser PJ, Marenco S, Pierpaoli C. Comprehensive approach for correction of motion and distortion in diffusion-weighted MRI. *Magn Reson Med* 2004; **51**(1): 103–114.
17. Jones DK, Basser PJ. ''Squashing peanuts and smashing pumpkins'': how noise distorts diffusion-weighted MR data. *Magn Reson Med* 2004; **52**(5): 979–993.
18. Pajevic S, Pierpaoli C. Color schemes to represent the orientation of anisotropic tissues from diffusion tensor data: application to white matter fiber tract mapping in the human brain. *Magn Reson Med* 1999; **42**(3): 526–540.
19. Mori S, Itoh R, Zhang J, Kaufmann WE, van Zijl PC, Solaiyappan M, Yarowsky P. Diffusion tensor imaging of the developing mouse brain. *Magn Reson Med* 2001; **46**(1): 18–23.
20. Klose U, Mader I, Unrath A, Erb M, Grodd W. Directional correlation in white matter tracks of the human brain. *J Magn Reson Imaging* 2004; **20**(1): 25–30.
21. Jonasson L, Bresson X, Hagmann P, Cuisenaire O, Meuli R, Thiran JP. White matter fiber tract segmentation in DT-MRI using geometric flows. *Med Image Anal* 2005; **9**(3): 223–236.
22. Pierpaoli C, Basser PJ. Toward a quantitative assessment of diffusion anisotropy. *Magn Reson Med* 1996; **36**(6): 893–906.
23. Constantinescu GM. *Clinical Dissection Guide for Large Animals*. Mosby-Year Book: St Louis, 1991: 334.
24. Baggett H, Doran GA. A structural and functional classification of mammalian tongues. *J Mammal* 1971; **52**(2): 427–429.
25. DePaul R, Abbs JH. Quantitative morphology and histochemistry of intrinsic lingual muscle fibers in Macaca fascicularis. *Acta Anat (Basel)* 1996; **155**(1): 29–40.
26. Damon BM, Ding Z, Anderson AW, Freyer AS, Gore JC. Validation of diffusion tensor MRI-based muscle fiber tracking. *Magn Reson Med* 2002; **48**(1): 97–104.

27. Jones DK. Determining and visualizing uncertainty in estimates of fiber orientation from diffusion tensor MRI. *Magn Reson Med* 2003; **49**(1): 7–12.

28. Kim S, Chi-Fishman G, Barnett AS, Pierpaoli C. Dependence on diffusion time of apparent diffusion tensor of ex vivo calf tongue and heart. *Magn Reson Med* 2005; **54**(6): 1387–1396.

29. Hsu J-J, Glover GH. Mitigation of susceptibility-induced signal loss in neuroimaging using localized shim coils. *Magn. Reson. Med.* 2005; **53**(2): 243–248.

30. Jaermann T, Crelier G, Pruessmann KP, Golay X, Netsch T, van Muiswinkel AM, Mori S, van Zijl PC, Valavanis A, Kollias S, Boesiger P. SENSE-DTI at 3 T. *Magn Reson Med* 2004; **51**(2): 230–236.